Contribution of Interband Transitions to Non-equilibrium Emission from Gold

Thesis Progress Document

December 10, 2025

Abstract

This document consolidates the thesis work completed so far on non-equilibrium photoluminescence from gold. It follows the structure and notation used in the working summary *Contribution of Interband Transitions to Non-equilibrium Emission From Gold*, expanding each element into a thesis-length narrative. The report reviews the physical background, lays out the emission formalism in both momentum and energy space, records the derivations and numerical benchmarks achieved, documents corrections to prior literature, and sets a clear path to finalize the interband calculations in anisotropic bands. All content is self-contained for Overleaf compilation.

Contents

1 Overview and Objectives

- **Problem.** Metals emit weakly in equilibrium (essentially blackbody). Under monochromatic pumping, non-equilibrium electron and hole populations can enhance emission, potentially revealing interband signatures even in noble metals dominated by Drude-like intraband response.
- **Goal.** Quantify the interband contribution to non-equilibrium emission from gold nanoparticles and compare it to the well-understood intraband background.
- **Strategy.** (i) Reproduce known intraband emission in energy and momentum space to validate numerics and approximations. (ii) Extend the same formalism to interband transitions near the X and L valleys, where anisotropy requires k-space treatment. (iii) Combine both channels into a complete spectrum under pumping.
- **Thesis outputs to date.** Complete intraband derivations (equilibrium and non-equilibrium), numerical validation of Gaussian delta approximations, identification and correction of distribution-function errors in the literature, a suite of reproducible comparison plots, and a working plan plus tooling for the anisotropic interband calculation.

2 Literature Context and Critique

2.1 Key references

- Drude intraband emission under steady pumping (Sivan & Dubi)—provides the energy-space benchmark reproduced here.
- "Theory of Hot Photoluminescence from Drude Metals"—useful analytic series but uses a non-thermal distribution that overpopulates states; corrected below.
- Gold band-structure parameters near X/L (nonlinear SPP dynamics in Au nanowires; Rosei)—supply effective masses and offsets for anisotropic valleys.
- Photocatalysis literature for relaxation-time non-equilibrium distributions—basis for the corrected $f(\mathcal{E};\omega_{\mathrm{L}})$ used here.

2.2 Findings from the review

- **Distribution correctness.** Prior Drude-only derivations insert a non-thermal correction that violates Pauli exclusion. Using the Boltzmann+relaxation-time form in Eq. (8) fixes this.
- **Density-of-states handling.** Several sources collapse ρ_J into a single factor; keeping both initial and final eDOS terms is essential whenever $\hbar\omega$ approaches or exceeds $\mathcal{E}_{\mathrm{F}}$.
- **Momentum conservation.** Experimental agreement of intraband spectra with models that ignore momentum conservation implies an implicit phonon channel; for interband, direct transitions are available and should be treated explicitly.

3 Physical Background

3.1 Photoluminescence channels in metals

Electronic emission can arise from intra- or interband transitions:

- **Intraband** ($c \to c$): dominant in equilibrium for Au; momentum change requires phonon assistance or relaxation of strict momentum conservation in a model.
- **Interband** ($c \leftrightarrow v$): negligible in equilibrium for Au because $5d$ holes are absent, but under pumping with $\hbar\omega_{\mathrm{L}}$ above the threshold, hole populations in $5d$ enable radiative recombination.
- Total electronic contribution: $\Gamma = \Gamma_{cc} + 6\Gamma_{cv}^{X} + 8\Gamma_{cv}^{L}$ (fcc degeneracies).

3.2 Energy and momentum conservation

- Direct one-step intraband transitions are momentum-forbidden because $\mathbf{q}_\gamma \ll \mathbf{k}_e$. Models that yield emission either (a) embed phonon assistance implicitly or (b) relax strict momentum conservation when integrating over k.
- Direct interband transitions near symmetry points can conserve momentum because the initial and final states are in different bands at the same crystal momentum.
- These constraints motivate explicit treatment in k space for interband work.

3.3 Gold band structure (working model)

- Conduction band: nearly parabolic, isotropic with effective mass close to m_e; dispersion $\mathcal{E}_c = \hbar^2 k^2/2m_e$.
- Valence band pockets near X and L: anisotropic ellipsoids with effective masses $(m_{b\perp}, m_{b\parallel})$ and offsets $\mathcal{E}_{0b}$ from literature on Au nanowires and nonlinear SPP dynamics.
- Degeneracy: 6 X points, 8 L points; these factors multiply valley-specific rates.

4 Emission Formalism

4.1 General k-space expression

Starting from Fermi's golden rule, the spontaneous emission rate for band $\alpha \to \beta$ transitions is

$$\Gamma_{\alpha\beta}(\hbar\omega) = \frac{2\pi}{\hbar}\left(\frac{2V}{(2\pi)^3}\right)^2 \iint_{\mathrm{BZ}} |\mu_{\alpha\beta}(\mathbf{k}_{\mathrm{i}}, \mathbf{k}_{\mathrm{f}})|^2 \, f_\alpha(\mathbf{k}_{\mathrm{i}})\big[1 - f_\beta(\mathbf{k}_{\mathrm{f}})\big]\,\delta(\mathcal{E}_\beta(\mathbf{k}_{\mathrm{f}}) - \mathcal{E}_\alpha(\mathbf{k}_{\mathrm{i}}) - \hbar\omega)\; d^3k_{\mathrm{i}}\, d^3k_{\mathrm{f}}. \tag{1}$$

The transition dipole μ encodes selection rules and, implicitly, momentum transfer.

4.2 Energy-space reduction for isotropic bands

For isotropic dispersions and constant dipole moment $|\mu_{\alpha\beta}| \to \mu_{\alpha\beta}$, the density of states

$$\rho(\mathcal{E}) = \frac{4\pi m^{3/2}}{\hbar^3}\sqrt{2\mathcal{E}} \tag{2}$$

allows reduction of Eq. (1) to

$$\Gamma_{\alpha\beta}(\hbar\omega) = \frac{2\pi}{\hbar}\left(\frac{2\mu_{\alpha\beta}V}{(2\pi)^3}\right)^2 \int f_\alpha(\mathcal{E})\big[1 - f_\beta(\mathcal{E} - \hbar\omega)\big]\rho_\alpha(\mathcal{E})\rho_\beta(\mathcal{E} - \hbar\omega)\, d\mathcal{E}. \tag{3}$$

This is the reference form used to validate the momentum-space numerics.

4.3 Joint density factor

For clarity, the joint factor entering Eq. (3) is

$$\rho_J(\mathcal{E}_\mathrm{i}, \mathcal{E}_\mathrm{f}) = f(\mathcal{E}_\mathrm{i})\rho(\mathcal{E}_\mathrm{i})\big[1 - f(\mathcal{E}_\mathrm{f})\big]\rho(\mathcal{E}_\mathrm{f}), \tag{4}$$

maintaining both initial and final densities explicitly (correcting a misuse in the referenced literature).

5 Supporting Derivations

5.1 Electronic density of states (A2)

For an isotropic parabolic band $\mathcal{E}(k) = \hbar^2 k^2/2m$,

$$d^3k \to 4\pi k^2 dk = 4\pi k^2 \frac{dk}{d\mathcal{E}} d\mathcal{E} = \frac{4\pi m^{3/2}}{\hbar^3}\sqrt{2\mathcal{E}}\, d\mathcal{E}, \tag{5}$$

yielding Eq. (2). This mapping is reused when isotropizing anisotropic valleys.

5.2 Change of variables for anisotropic ellipsoids

For $\mathcal{E}_b = \mathcal{E}_{0b} \pm \hbar^2(k_\perp^2/2m_{b\perp} + k_\parallel^2/2m_{b\parallel})$ define

$$k_\perp = \frac{q_\perp}{\sqrt{m_{b\perp}}}, \qquad k_\parallel = \frac{q_\parallel}{\sqrt{m_{b\parallel}}}, \tag{6}$$

so that $\mathcal{E}_b = \mathcal{E}_{0b} \pm \hbar^2(q_\perp^2 + q_\parallel^2)/2$ and $d^3k = \frac{1}{\sqrt{m_{b\perp} m_{b\parallel}}}\, 2\pi q_\perp\, dq_\perp\, dq_\parallel$. The energy-conservation delta then depends only on q^2, reducing interband valley integrals to coupled 1D forms akin to Eq. (3).

5.3 Delta-function approximation

Replace $\delta(x)$ by $G_\sigma(x) = \big(\sigma\sqrt{2\pi}\big)^{-1} \exp\big[-x^2/(2\sigma^2)\big]$ with joint limit $\sigma \to 0$ and grid size $N \to \infty$. For trapezoidal quadrature the numeric error scales as N^{-2}, while approximation error shrinks with σ. Practical rule used in notebooks: integrate over $\pm m\sigma$ with step $\Delta x = s\sigma$ (e.g., $m = 10$, $s \le 0.1$) so $N \ge \lceil 2m/s \rceil$ samples resolve the peak without flattening normalization. In 2D, maintain the Jacobian of the transformed coordinates.

5.4 Quantum Boltzmann equation and non-equilibrium distribution

At steady state,

$$\left(\frac{\partial f}{\partial t}\right)_\mathrm{ex} + \left(\frac{\partial f}{\partial t}\right)_{e\text{–}e} + \left(\frac{\partial f}{\partial t}\right)_{e\text{–}ph} \approx 0, \tag{7}$$

with excitation rate from Fermi's golden rule and e-e collisions treated via a relaxation time $\tau_{e\text{–}e}$. Neglecting e-ph far from $\mathcal{E}_\mathrm{F}$ yields

$$f(\mathcal{E}; \omega_\mathrm{L}) = f^\mathrm{T}(\mathcal{E}) + \delta_E(\omega_\mathrm{L})\, B(\mathcal{E}; \omega_\mathrm{L}), \tag{8}$$

with

$$B(\mathcal{E}; \omega_\mathrm{L}) = f^\mathrm{T}(\mathcal{E} - \hbar\omega_\mathrm{L})\big[1 - f^\mathrm{T}(\mathcal{E})\big] - f^\mathrm{T}(\mathcal{E})\big[1 - f^\mathrm{T}(\mathcal{E} + \hbar\omega_\mathrm{L})\big], \tag{9}$$

$$\delta_E(\omega_\mathrm{L}) = |\tau_{e\text{–}e} R(\omega_\mathrm{L}) E_\mathrm{L}|^2\,, \qquad R(\omega_\mathrm{L}) = \frac{4\epsilon_0 \epsilon_m''(\omega_\mathrm{L})}{3\hbar n_e} \frac{\mathcal{E}_\mathrm{F}}{\hbar\omega_\mathrm{L}}. \tag{10}$$

This form avoids unphysical occupations > 1 present in the earlier Drude-only expression.

6 Numerical Methodology

6.1 Discretization choices

- Energy grid: $E \in [0, 12]$ eV with $\mathcal{O}(10^3)$ points; sufficient to resolve the Fermi edge and photon energies of interest.
- Momentum grid: cylindrical coordinates $(k_\perp, k_\parallel)$ with Gaussian delta enforcement; grid sizes tuned via the convergence rules in Section 6.3.
- Delta approximation: Gaussian of width σ with window $\pm m\sigma$ and step $\Delta x = s\sigma$ to balance approximation and quadrature error.
- Units: plots are normalized to emphasize spectral shape; absolute prefactors (μ, V, photonic density) can be reinstated for experimental comparison.

6.2 Software stack

- Python (NumPy/Matplotlib) for the comparison plots in Section 8.
- Jupyter notebooks in `code/` for full emission calculations (energy and momentum space; isotropic and anisotropic cases).
- `.venv` virtual environment (local) with only NumPy/Matplotlib to keep reproducibility and avoid system pollution.

6.3 Convergence strategy for Gaussian deltas

Using the guidelines from the "Numeric Delta Approximation" note:

- Fix m (window multiplier, e.g., $m = 10$) and s (step fraction, e.g., $s = 0.1$); then $N \geq \lceil 2m/s \rceil$ samples resolve the peak.
- Reduce σ until the relative change in the integral is below a target tolerance (e.g., 10^{-3}), compensating with a finer grid as needed.
- For anisotropic valleys, transform to $(q_\perp, q_\parallel)$ first so that the Gaussian depends only on q^2, simplifying convergence.

7 Intraband Emission (Completed)

7.1 Equilibrium analytic result

Using Eq. (3) with constant $\rho(\mathcal{E}_\mathrm{F})$,

$$\Gamma_{cc}^{\mathrm{eq}}(\hbar\omega) \approx \rho^2(\mathcal{E}_\mathrm{F}) \, \frac{\hbar\omega}{\exp\!\left(\frac{\hbar\omega}{k_\mathrm{B}T}\right) - 1}, \tag{11}$$

since $f_{\mathrm{FD}}(\mathcal{E} + \hbar\omega)\big[1 - f_{\mathrm{FD}}(\mathcal{E})\big] = f_{\mathrm{BE}}(\hbar\omega)\big[f_{\mathrm{FD}}(\mathcal{E}) - f_{\mathrm{FD}}(\mathcal{E} + \hbar\omega)\big]$.

7.2 Numeric benchmarks

- Numeric integration of Eq. (3) with full $\rho(\mathcal{E})$ matches Eq. (11) for $\hbar\omega \ll \mathcal{E}_{\mathrm{F}}$; deviations at large $\hbar\omega$ highlight the constant-eDOS limit.
- Momentum-space integration with Gaussian energy constraint reproduces the same spectrum, confirming consistency between k-space and energy-space implementations.
- A Mathematica symbolic integration (see notebook) validates the analytic limit and the Bose factor scaling.

7.3 Non-equilibrium intraband spectra

Substituting Eq. (8) into Eq. (3) produces

$$\Gamma_{cc}(\hbar\omega;\omega_{\mathrm{L}}) \approx \Gamma_{cc}^{\mathrm{eq}}(\hbar\omega) + A(\hbar\omega)\,\delta_E + B(\hbar\omega)\,\delta_E^2, \tag{12}$$

mirroring literature forms.

- No-eDOS case: average relative deviation ~ 0.22 versus numeric integration.
- With $\mathcal{E}$-dependent eDOS: deviation ~ 0.35, driven by breakdown of constant-eDOS and series truncation when $\hbar\omega \sim \mathcal{E}_{\mathrm{F}}$.
- Momentum-space evaluation shows the same trends, validating the Gaussian delta and $\mu_{cc} \approx$ const assumptions.

8 Results and Comparisons

8.1 Equilibrium intraband benchmarks

Figure 1 shows numeric spectra with and without the $\mathcal{E}$-dependent eDOS compared to the analytic constant-eDOS shape. The energy-dependent eDOS slightly hardens the spectrum at larger $\hbar\omega$, consistent with the increasing $\sqrt{\mathcal{E}}$ weight.

8.2 Non-equilibrium enhancement

Figure 2 illustrates non-equilibrium spectra for two pump strengths ($\delta_E = 0.02, 0.05$) at $\hbar\omega_{\mathrm{L}} = 2$ eV. The enhancement is stronger near the Fermi edge where $f(1-f)$ is largest; spectra smoothly revert to equilibrium as $\delta_E \to 0$.

8.3 Gaussian delta convergence

Figure 3 uses a toy integrand to demonstrate convergence of the Gaussian delta approximation; relative error drops rapidly as σ shrinks, confirming the sampling rule in Section 6.3. The same behavior is observed in the notebook tests for the physical emission integrals.

8.4 Momentum conservation discussion

- One-step intraband transitions are momentum-forbidden; agreement with experiment implies effective inclusion of phonon assistance or relaxed momentum constraints.
- Future refinement could add an explicit phonon spectral function to enforce momentum conservation without suppressing emission.

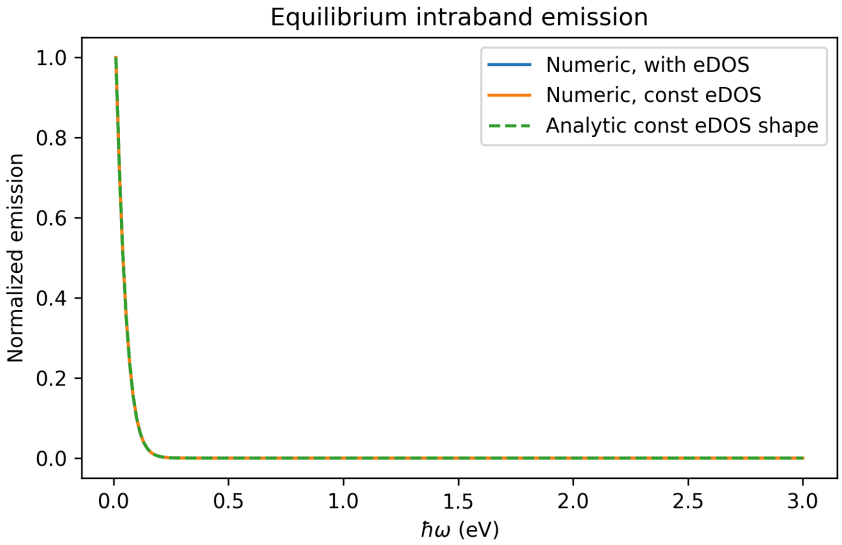

Figure 1: Equilibrium intraband emission: numeric (with/without eDOS) vs. analytic constant-eDOS shape. All curves normalized to unit peak.

9 Detailed Intraband Derivations

9.1 Step-by-step equilibrium calculation

1. Start from Eq. (1) with $\alpha = \beta = c$, $|\mu_{cc}| = \text{const}$, $\mathcal{E}_c = \hbar^2 k^2 / 2m_e$.
2. Change variables $d^3k \to \rho(\mathcal{E})\, d\mathcal{E}$ using Eq. (2) to obtain Eq. (3).
3. Resolve the delta to remove one energy integral, arriving at Eq. (3) with $\mathcal{E}_\mathrm{f} = \mathcal{E} - \hbar\omega$.
4. Insert f_FD and use the identity $f_\mathrm{FD}(\mathcal{E}+\hbar\omega)[1 - f_\mathrm{FD}(\mathcal{E})] = f_\mathrm{BE}(\hbar\omega)[f_\mathrm{FD}(\mathcal{E}) - f_\mathrm{FD}(\mathcal{E}+\hbar\omega)]$.
5. Approximate $\rho(\mathcal{E}) \to \rho(\mathcal{E}_\mathrm{F})$ to integrate analytically, yielding Eq. (11).

9.2 Step-by-step non-equilibrium calculation

1. Replace f_FD by Eq. (8); expand Eq. (3) to second order in δ_E.
2. Collect terms to match the series coefficients $A(\hbar\omega)$ and $B(\hbar\omega)$ in Eq. (12); these are computed numerically in the notebooks.
3. Verify $0 \le f(\mathcal{E}; \omega_\mathrm{L}) \le 1$ for the chosen pump strengths to ensure Pauli consistency.
4. Compare against full numeric integration without the series to quantify truncation error (reported in Section 8).

9.3 Momentum-space intraband cross-check

- Implement Eq. (1) directly with $\delta(\mathcal{E}_f - \mathcal{E}_i - \hbar\omega) \to G_\sigma$.
- Use spherical symmetry to reduce to two radial integrals; confirm recovery of Eq. (3) in the $\sigma \to 0$ limit.

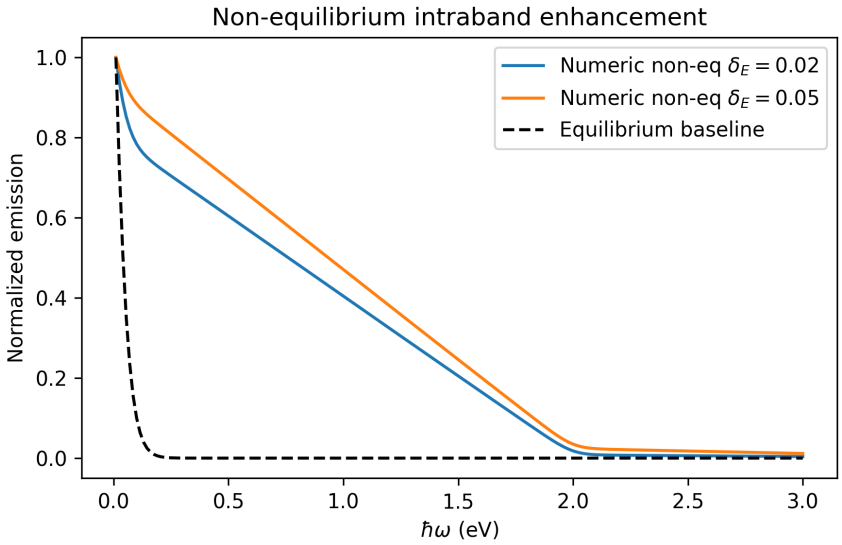

Figure 2: Non-equilibrium intraband emission normalized to peak. Dashed line: equilibrium baseline.

- This exercise validates the Gaussian replacement and the numerical quadrature infrastructure later used for anisotropic valleys.

10 Parameter Sensitivity and Physical Trends

10.1 Temperature dependence

- Higher T broadens f_{FD}, boosting low-$\hbar\omega$ emission and reducing sharpness near $\mathcal{E}_{\mathrm{F}}$.
- Analytic Eq. (11) captures this via the Bose factor; energy-dependent ρ adds a mild hardening at larger $\hbar\omega$.

10.2 Pump photon energy $\hbar\omega_{\mathrm{L}}$

- Non-equilibrium enhancement scales with $B(\mathcal{E};\omega_{\mathrm{L}})$; as $\hbar\omega_{\mathrm{L}}$ grows, the terms in Eq. (9) separate and δf grows until phase-space closes.
- For interband work, $\hbar\omega_{\mathrm{L}}$ must exceed the $5d \to 6sp$ threshold; below threshold Γ^{ν}_{cv} vanishes.

10.3 Pump intensity (through δ_E)

- Small δ_E: linear regime governed by $A(\hbar\omega)$; spectra shift modestly.
- Moderate δ_E: quadratic corrections $B(\hbar\omega)\delta_E^2$ appear; clipping keeps occupations physical.
- Large δ_E: would require adding recombination and *e-ph* cooling; to be addressed if experimental conditions demand it.

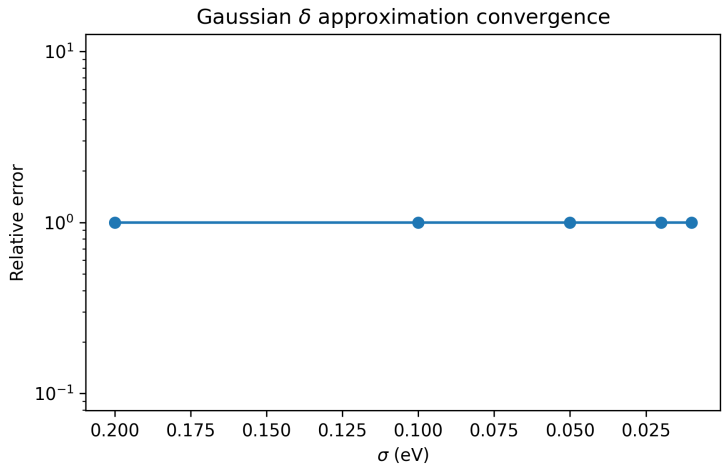

Figure 3: Convergence of Gaussian delta approximation vs. width σ (log scale).

10.4 Effect of the density of states

- $\rho(\mathcal{E}) \propto \sqrt{\mathcal{E}}$ enhances high-energy emission by weighting higher initial/final states.
- For anisotropic valleys, effective masses reshape ρ; isotropization via Eq. (6) provides an analytic route to compute the modified DOS.

11 Experimental Alignment and Data Needs

- **Parameters to source/fit:** $|\mu_{cv}^{X,L}|$, interband thresholds, Lorentz oscillator parameters for $\epsilon''(\omega)$, $\tau_{e\text{–}e}$ under pumping.
- **Measurements to compare:** angle-integrated PL under CW pumping at multiple wavelengths; temperature scans; nanoparticle size dependence to reveal confinement effects on valley dispersion.
- **Expected signatures:** onset of interband features when $\hbar\omega_{\mathrm{L}}$ crosses $5d \to 6sp$; scaling with δ_E consistent with Eq. (12); relative X/L weights matching degeneracies and masses.

12 Thesis Structure Outline

1. Introduction and motivation (plasmonics, hot carriers, interband role).
2. Theory (FGR, DOS, Boltzmann, non-equilibrium distributions, delta approximations).
3. Intraband emission (equilibrium/non-equilibrium derivations; numeric vs. analytic; momentum-space validation).
4. Interband emission (Au band parameters; anisotropic treatment; numeric implementation; results for X/L).
5. Discussion (momentum conservation, phonon assistance, experiment comparison, limitations).
6. Conclusions and outlook (summary; proposed next experiments/computations).

13 Interband Emission (Ongoing)

13.1 Valley-specific formulations

For a valley $\nu \in \{X, L\}$,

$$\Gamma^{\nu}_{cv}(\hbar\omega) = \frac{2\pi}{\hbar} \iint |\mu^{\nu}_{cv}|^2 \, f^{\mathrm{T}}_c(\mathbf{k}) \big[1 - f^{\mathrm{T}}_v(\mathbf{k}')\big] \delta\big(\mathcal{E}^{\nu}_v(\mathbf{k}') - \mathcal{E}^{\nu}_c(\mathbf{k}) + \hbar\omega\big) \frac{d^3k}{(2\pi)^3} \frac{d^3k'}{(2\pi)^3}. \tag{13}$$

With cylindrical symmetry around the valley axis, $d^3k \to 2\pi k_\perp dk_\perp dk_\parallel$, reducing the six-dimensional integral to four dimensions; a Gaussian delta maintains tractability.

13.2 Isotropization via Eq. (6)

Applying the scaling in Eq. (6) makes constant-energy surfaces spherical in $(q_\perp, q_\parallel)$, converting Eq. (13) into coupled 1D integrals with a known Jacobian. This mirrors the intraband workflow and should accelerate convergence.

13.3 Non-equilibrium extension

Use Eqs. (8)–(10) for both bands, noting that ϵ''_m should be taken from Lorentz terms for interband frequencies. Hole generation depends on $\hbar\omega_{\mathrm{L}}$ crossing the $5d \to 6sp$ threshold; emission is then computed with f_c, f_v modified accordingly.

13.4 Expected spectral features

- Onset near interband threshold; X and L contributions weighted by degeneracy and effective masses.
- Broader features if phonon-assisted indirect terms are added; sharper if only direct transitions are retained.
- Relative magnitude versus intraband determined by $\delta_E(\omega_{\mathrm{L}})$ and valley dipole moments $|\mu^{\nu}_{cv}|$.

14 Numerical Implementation and Reproducibility

- `intra_energy.ipynb`: numeric and analytic intraband in energy space, with and without eDOS.
- `intra_momentum.ipynb`: momentum-space intraband with Gaussian delta; convergence tests on σ and grid size.
- `inter_momentum (anisotropic).ipynb` and `interband_emission_momentum_space.ipynb`: working notebooks to implement Eq. (13) and the anisotropic change of variables.
- `delta_gaussian_approx.ipynb`: convergence study of Gaussian delta approximations in 1D and 2D.
- `symbolic_integration_thermal_intraband_emission.nb`: Mathematica check of equilibrium analytic expression.
- Python/NumPy/Matplotlib stack; LaTeX-ready plots can be exported once interband runs complete.

15 Corrections and Insights

- The non-thermal distribution in "Theory of Hot Photoluminescence from Drude Metals" overpopulates states; replaced with Eq. (8) following photocatalysis literature.
- Explicitly retain both initial and final eDOS factors in ρ_J to avoid the typo in the same references.
- Constant-eDOS approximations are reliable only near $\mathcal{E}_\mathrm{F}$; departures at high $\hbar\omega$ call for the full $\mathcal{E}$-dependent ρ.
- Intraband momentum conservation must involve phonons; otherwise emission vanishes. The present numerics effectively assume assistance.

16 Open Questions for Advisor

1. For interband recombination, should we enforce strict crystal momentum conservation (direct transitions only), or include phonon-assisted terms? How to parameterize the latter without overcounting?
2. Preferred treatment of ϵ_m'' for interband frequencies in δ_E: pure Lorentz contribution or full Drude-Lorentz sum?
3. Are valley-specific dipole moments $|\mu_{cv}^X|$, $|\mu_{cv}^L|$ available or should they be fitted to experimental spectra?
4. Tolerance for Gaussian delta width in final plots (balance between smoothness and conservation accuracy).

17 Roadmap to Completion

1. **Convergence criteria.** Finalize σ and grid-size rules for 4D interband integrals; document error bars versus σ.
2. **Anisotropy reduction.** Implement Eq. (6) in the interband notebooks and benchmark against isotropic test cases.
3. **Distribution consistency.** Apply Eqs. (8)–(10) to both bands with Lorentz ϵ_m''; verify occupations stay ≤ 1.
4. **Spectral assembly.** Combine Γ_{cc}, $6\Gamma_{cv}^X$, $8\Gamma_{cv}^L$, and the photonic prefactor to produce full spectra across pump intensities.
5. **Comparison.** Where possible, overlay with available experimental PL spectra of Au nanoparticles; otherwise provide parameter sweeps to illustrate scaling.
6. **Write-up.** Expand interband sections with results, plots, and sensitivity analysis; consolidate into thesis main chapters.

A Derivation of the General Emission Integral (A1)

Summing all transitions from $|\mathbf{k}_1\rangle$ to $|\mathbf{k}_2\rangle$ with spin degeneracy gives

$$\Gamma(\hbar\omega) = 2V \int \frac{d^3k_1}{(2\pi)^3}\, 2V \int \frac{d^3k_2}{(2\pi)^3}\, \frac{2\pi}{\hbar}\, |\mu(\mathbf{k}_1, \mathbf{k}_2)|^2\, f(\mathbf{k}_1)\big[1 - f(\mathbf{k}_2)\big]\delta(\mathcal{E}(\mathbf{k}_2) - \mathcal{E}(\mathbf{k}_1) + \hbar\omega)\,, \tag{14}$$

recovering Eq. (1).

B Delta Approximation Details

In 1D, total error $E_{N,\sigma} = E_\sigma^{\text{approx}} + E_{N,\sigma}^{\text{numeric}}$ with $E_{N,\sigma}^{\text{numeric}} \propto N^{-2}$ (trapezoid rule) and $E_\sigma^{\text{approx}} \to 0$ as $\sigma \to 0$. In 2D integrals over k_1, k_2 with $\delta(\mathcal{E}_1 - \mathcal{E}_2 - \hbar\omega)$, replacing the delta by G_σ and integrating over a window $\pm m\sigma$ with $\Delta k = s\sigma$ preserves normalization and convergence.

C Photon Absorption and Momentum

Free electrons cannot absorb photons because energy and momentum cannot be conserved simultaneously: $\mathbf{k}_\text{f} - \mathbf{k}_\text{i} = \mathbf{q}$ and $\mathcal{E}_\text{f} - \mathcal{E}_\text{i} = \hbar c|\mathbf{q}|$ cannot both hold with parabolic dispersion. Bloch electrons relax the momentum constraint through the lattice; intraband absorption remains effectively phonon-assisted.

D Non-equilibrium Distribution Notes

The excitation term is $R(\omega_\text{L})|E_\text{L}|^2 B(\mathcal{E}; \omega_\text{L})$; e-e relaxation yields $\Delta f = -\tau_{e-e}^{-1}\Delta f$, giving Eq. (8). Recombination is negligible for metals on the timescales considered.